Acknowledgments

This work was supported by a Grant-in-Aid for Scientific Research on Priority Areas from the Ministry of Education, Culture, Sports, Science and Technology of Japan (20014015 to H.T), and Grants-in-Aid for Scientific Research (23300363 and 23650626 to H.T) from Hiroshima University.

Disclosures

H.T is a founder and the board director of MiRTeL Inc, and owns stock of MiRTeL Inc.

References

1. Makarov VL, Hirose Y, Langmore JP: Long G tails at both ends of human chromosomes suggest a C strand degradation mechanism for telomere shortening. *Cell* 88: 657–666, 1997
2. de Lange T: T-loops and the origin of telomeres. *Nat Rev Mol Cell Biol* 5: 323–329, 2004
3. Blasco MA: Mice with bad ends: Mouse models for the study of telomeres and telomerase in cancer and aging. *EMBO J* 24: 1095–1103, 2005
4. Stewart SA, Ben-Porath I, Carey VJ, O'Connor BF, Hahn WC, Weinberg RA: Erosion of the telomeric single-strand overhang at replicative senescence. *Nat Genet* 33: 492–496, 2003
5. Anno K, Hayashi A, Takahashi T, Mitsui Y, Ide T, Tahara H: Telomerase activation induces elongation of the telomeric single-stranded overhang, but does not prevent chromosome aberrations in human vascular endothelial cells. *Biochem Biophys Res Commun* 353: 926–932, 2007
6. Cawthon RM, Smith KR, O'Brien E, Sivatchenko A, Kerber RA: Association between telomere length in blood and mortality in people aged 60 years or older. *Lancet* 361: 393–395, 2003
7. Guan JZ, Maeda T, Sugano M, Oyama J, Higuchi Y, Makino N: Change in the telomere length distribution with age in the Japanese population. *Mol Cell Biochem* 304: 353–360, 2007
8. Benetos A, Okuda K, Lajemi M, Kimura M, Thomas F, Skurnick J, Labat C, Bean K, Aviv A: Telomere length as an indicator of biological aging: The gender effect and relation with pulse pressure and pulse wave velocity. *Hypertension* 37: 381–385, 2001
9. Epel ES, Merkin SS, Cawthon R, Blackburn EH, Adler NE, Pletcher MJ, Seeman TE: The rate of leukocyte telomere shortening predicts mortality from cardiovascular disease in elderly men. *Aging (Albany, NY Online)* 1: 81–88, 2009
10. Carrero JJ, Stenvinkel P, Fellström B, Qureshi AR, Lamb K, Heimbürger O, Bárány P, Radhakrishnan K, Lindholm B, Soveri I, Nordfors L, Shiels PG: Telomere attrition is associated with inflammation, low fetuin-A levels and high mortality in prevalent haemodialysis patients. *J Intern Med* 263: 302–312, 2008
11. Ramírez R, Carracedo J, Soriano S, Jiménez R, Martín-Malo A, Rodríguez M, Blasco M, Aljama P: Stress-induced premature senescence in mononuclear cells from patients on long-term hemodialysis. *Am J Kidney Dis* 45: 353–359, 2005
12. Tsirpanlis G, Chatzipanagiotou S, Boufidou F, Kordinas V, Alevyzaki F, Zoga M, Kyritsis I, Stamatelou K, Triantafyllis G, Nicolaou C: Telomerase activity is decreased in peripheral blood mononuclear cells of hemodialysis patients. *Am J Nephrol* 26: 91–96, 2006
13. Schiffrin EL, Lipman ML, Mann JF: Chronic kidney disease: Effects on the cardiovascular system. *Circulation* 116: 85–97, 2007
14. Wills LP, Schnellmann RG: Telomeres and telomerase in renal health. *J Am Soc Nephrol* 22: 39–41, 2011
15. Tahara H, Kusunoki M, Yamanaka Y, Matsumura S, Ide T: G-tail telomere HPA: Simple measurement of human single-stranded telomeric overhangs. *Nat Methods* 2: 829–831, 2005
16. Tahara H: Telomere G-overhang length measurement method 2: G-tail telomere HPA. *Methods Mol Biol* 735: 55–61, 2011
17. Payne RB, Little AJ, Williams RB, Milner JR: Interpretation of serum calcium in patients with abnormal serum proteins. *BMJ* 4: 643–646, 1973
18. Daugirdas JT: Second generation logarithmic estimates of single-pool variable volume Kt/V: an analysis of error. *J Am Soc Nephrol* 4:1205–1213, 1993
19. Nakai S, Suzuki K, Masakane I, Wada A, Itami N, Ogata S, Kimata N, Shigematsu T, Shinoda T, Syouji T, Taniguchi M, Tsuchida K, Nakamoto H, Nishi S, Nishi H, Hashimoto S, Hasegawa T, Hanafusa N, Hamano T, Fujii N, Marubayashi S, Morita O, Yamagata K, Wakai K, Watanabe Y, Iseki K, Tsubakihara Y: Overview of regular dialysis treatment in Japan (as of 31 December 2008). *Ther Apher Dial* 14: 505–540, 2010
20. Houben JM, Moonen HJ, van Schooten FJ, Hageman GJ: Telomere length assessment: Biomarker of chronic oxidative stress? *Free Radic Biol Med* 44: 235–246, 2008
21. Ogami M, Ikura Y, Ohsawa M, Matsuo T, Kayo S, Yoshimi N, Hai E, Shirai N, Ehara S, Komatsu R, Naruko T, Ueda M: Telomere shortening in human coronary artery diseases. *Arterioscler Thromb Vasc Biol* 24: 546–550, 2004
22. Fyhrquist F, Saijonmaa O: Telomere length and cardiovascular aging. *Ann Med* 44[Suppl 1]: S138–S142, 2012
23. Epel ES, Blackburn EH, Lin J, Dhabhar FS, Adler NE, Morrow JD, Cawthon RM: Accelerated telomere shortening in response to life stress. *Proc Natl Acad Sci U S A* 101: 17312–17315, 2004
24. Tahara H, Shin-Ya K, Seimiya H, Yamada H, Tsuruo T, Ide T: G-Quadruplex stabilization by telomestatin induces TRF2 protein dissociation from telomeres and anaphase bridge formation accompanied by loss of the 3′ telomeric overhang in cancer cells. *Oncogene* 25: 1955–1966, 2006
25. Markkanen E, van Loon B, Ferrari E, Parsons JL, Dianov GL, Hübscher U: Regulation of oxidative DNA damage repair by DNA polymerase λ and MutYH by cross-talk of phosphorylation and ubiquitination. *Proc Natl Acad Sci U S A* 109: 437–442, 2012
26. de Lange T: Shelterin: The protein complex that shapes and safeguards human telomeres. *Genes Dev* 19: 2100–2110, 2005
27. Betjes MG, Langerak AW, van der Spek A, de Wit EA, Litjens NH: Premature aging of circulating T cells in patients with end-stage renal disease. *Kidney Int* 80: 208–217, 2011
28. Menon MC, Ix JH: Dietary phosphorus, serum phosphorus, and cardiovascular disease. *Ann N Y Acad Sci* 1301: 21–26, 2013
29. Block GA, Klassen PS, Lazarus JM, Ofsthun N, Lowrie EG, Chertow GM: Mineral metabolism, mortality, and morbidity in maintenance hemodialysis. *J Am Soc Nephrol* 15: 2208–2218, 2004
30. Cherkas LF, Hunkin JL, Kato BS, Richards JB, Gardner JP, Surdulescu GL, Kimura M, Lu X, Spector TD, Aviv A: The association between physical activity in leisure time and leukocyte telomere length. *Arch Intern Med* 168: 154–158, 2008
31. Lin KW, Yan J: The telomere length dynamic and methods of its assessment. *J Cell Mol Med* 9: 977–989, 2005

Received: September 30, 2013 **Accepted:** August 20, 2014

Published online ahead of print. Publication date available at www.cjasn.org.

This article contains supplemental material online at http://cjasn.asnjournals.org/lookup/suppl/doi:10.2215/CJN.10010913/-/DCSupplemental.

Published OnlineFirst May 29, 2014; DOI: 10.1158/0008-5472.CAN-13-3604

Therapeutics, Targets, and Chemical Biology

Cancer Research

CBP-93872 Inhibits NBS1-Mediated ATR Activation, Abrogating Maintenance of the DNA Double-Strand Break–Specific G_2 Checkpoint

Takahisa Hirokawa[1,2], Bunsyo Shiotani[3], Midori Shimada[1], Kazuhiro Murata[1], Yoshikazu Johmura[1], Mayumi Haruta[1], Hidetoshi Tahara[3], Hiromitsu Takeyama[2], and Makoto Nakanishi[1]

Abstract

CBP-93872 was previously identified as a G_2 checkpoint inhibitor using a cell-based high-throughput screening system. However, its molecular actions as well as cellular targets are largely unknown. Here, we uncovered the molecular mechanisms underlying abrogation of the G_2 checkpoint by CBP-93872. CBP-93872 specifically abrogates the DNA double-stranded break (DSB)–induced G_2 checkpoint through inhibiting maintenance but not initiation of G_2 arrest because of specific inhibition of DSB-dependent ATR activation. Hence, ATR-dependent phosphorylation of Nbs1 and replication protein A 2 upon DSB was strongly suppressed in the presence of CBP-93872. CBP-93872 did not seem to inhibit DNA-end resection, but did inhibit Nbs1-dependent and ssDNA-induced ATR activation *in vitro* in a dose-dependent manner. Taken together, our results suggest that CBP-93872 is an inhibitor of maintenance of the DSB-specific G_2 checkpoint and thus might be a strong candidate as the basis for a drug that specifically sensitizes p53-mutated cancer cells to DSB-inducing DNA damage therapy. *Cancer Res; 74(14); 3880–9. ©2014 AACR.*

Introduction

Maintaining the genomic stability of both normal cells and cancer cells depends on coordinated networks of different forms of the DNA damage response, which execute various cell activities such as cell-cycle arrest, apoptosis, and premature senescence (1). Abrogation of these systems likely leads to extensive genomic instability and subsequent cell death upon DNA damage. Cell-cycle arrest in response to DNA damage plays a key role in increasing cell survival and is mediated in mammals by at least two distinct pathways; one via ATM-p53-p21 (2, 3) and the other via ATM/ATR-Chk1-Cdc25 (4, 5). The former mediates both G_1 and G_2 arrest and the latter mediates G_2 arrest (6–8). Given that most cancer cells have genetic alterations in p53, their survival in the presence of DNA damage depends on a functional Chk1-mediated G_2 checkpoint, suggesting that reagents capable of inhibiting this checkpoint would be promising drugs for producing synthetic lethality to p53-deficient cancer cells.

Authors' Affiliations: Departments of [1]Cell Biology and [2]Gastroenterological Surgery, Graduate School of Medical Sciences, Nagoya City University, Mizuho-cho, Mizuho-ku, Nagoya; and [3]Department of Cellular and Molecular Biology, Hiroshima University, Hiroshima, Japan

Note: Supplementary data for this article are available at Cancer Research Online (http://cancerres.aacrjournals.org/).

Corresponding Author: Makoto Nakanishi, Department of Cell Biology, Graduate School of Medical Sciences, Nagoya City University, 1 Kawasumi, Mizuho-cho, Mizuho-ku, Nagoya 467-8601, Japan. Phone: 81-52-853-8144; Fax: 81-52-842-3955; E-mail: mkt-naka@med.nagoya-cu.ac.jp

doi: 10.1158/0008-5472.CAN-13-3604

Signals initiated by DNA damage sensors are rapidly transduced to downstream targets in a manner dependent on the type of damage. For example, signals from DNA double-stranded break (DSB) sensors are rapidly transduced to an ataxia telangiectasia mutated (ATM) kinase (9) and a DNA-dependent protein kinase catalytic subunit (DNA-PKcs) that in turn leads to the processing of DSBs by nucleases generating an ATR-activating structure (10–12). In contrast, a broad spectrum of DNA damage changes, such as a structure consisting of single-stranded DNA (ssDNA) and a junction between ssDNA and double-stranded DNA (dsDNA), can directly activate ATM- and Rad3-related (ATR) kinases in a replication protein A (RPA)- and Rad17-dependent manner, respectively (13). The activated ATM and/or ATR transduce the damage signals to a large number of downstream effectors, such as p53, Chk1, and Chk2, and execute G_1 and G_2 DNA damage checkpoints (1).

On the basis of the absolute requirement for the G_2 DNA damage checkpoint for p53-deficient cancer cell survival upon DNA damage, various G_2 checkpoint inhibitors have been developed and proposed for clinical application. Among them, caffeine is one of the most extensively investigated agents that inhibits ATM and ATR kinases and increases sensitization of p53-deficient cells to IR irradiation. Chk1 inhibitors, such as UCN-01 (14), CEP-3891 (15), and AZD7762 (16) are also proposed to be potent G_2 checkpoint suppressors. However, the kinases ATR and Chk1 are essential for mammalian cell survival (17–21) and ATM is also required for maintaining genomic integrity during normal cell growth (22). Therefore, these drugs would have unexpected deleterious effects on normal cell function, diminishing the possibility of their clinical application.

Published OnlineFirst May 29, 2014; DOI: 10.1158/0008-5472.CAN-13-3604

We have previously identified CBP-93872 as a promising G_2 checkpoint inhibitor using a high-throughput screening system that detected abrogation of the G_2 checkpoint in IR-irradiated HT-29 cells (23). However, molecular mechanisms underlying G_2 checkpoint inhibition by this drug are largely unknown. Importantly, treatment with this drug markedly sensitized p53-mutated cancer cells to DSB-inducing DNA damaging agents. In this study, we investigated the molecular basis of G_2 checkpoint inhibition by CBP-93872 in p53-deficient cancer cells and found that CBP-93872 specifically inhibited DSB-mediated and Nbs1-dependent activation of ATR.

Materials and Methods

Cell culture and drug treatment

HT29 and HCT116 cells were grown in McCoy's 5A (Gibco) supplemented with 10% fetal bovin serum (FBS) and 1% penicillin–streptomycin (Invitrogen). NCI-H460, A549 and MCF7 cells were cultured in RPMI-1640 (Sigma-Aldrich) supplemented with 10% FBS and 1% penicillin–streptomycin. All cells were cultured at 37 °C under 5% CO_2.

Inhibitors used in this study were as follows: CBP-93872 (20 μmol/L; kindly supplied by Chugai Pharmaceutical Co., Ltd.), UCN01 (300 nmol/L; Sigma-Aldrich), caffeine (2 mmol/L; Sigma-Aldrich), KU-55933 (20 μmol/L; Sigma-Aldrich), and Nocodazole (500 nmol/L; Sigma-Aldrich).

MMS (Sigma-Aldrich) was used at 200 μmol/L and hydroxyurea (Sigma-Aldrich) was used at different concentrations.

Plasmid construction

To generate lentivirus shRNA constructs, an shRNA-coding fragment with a 5′-ACGTGTGCTGTCCGT-3′ loop was digested into pENTER4-H1tetOx1 (a gift of H. Miyoshi). To insert the H1tetOx1-shRNA into a lentivirus vector, the vector pENTER4-H1tetOx1-shRNA was mixed with CS-RFA-ETBsd (a gift of H. Miyoshi) and treated with Gateway LR clonase (Invitrogen).

The full-length cDNA of wild-type human Nbs1 was obtained by RT-PCR, and ligated into pcDNA3.1-myc-His vector. To construct Tet-on inducible lentivirus vectors, a cDNA fragment of Nbs1 containing the myc-His epitope was inserted into a pENTER1A vector (Invitrogen). shRNA-resistant mutations and an EDE mutation of pENTR1A Nbs1-myc-His were generated by inverse PCR with a Site-Specific Mutagenesis Kit (Toyobo). The resultant plasmids were mixed with CS-IV-TRE-RfA-UbC-Puro vector (a gift of H. Miyoshi), and treated with Gateway LR clonase to generate the lentivirus vectors.

Virus generation and infection

Lentiviruses expressing the respective shRNAs were generated by cotransfection of 293T cells with pCMV-VSV-G-RSV-RevB (a gift of H. Miyoshi), pCAG-HIVgp (a gift of H. Miyoshi), and the respective CS-RFA-ETBsd using the calcium phosphate coprecipitation method. HT29 cells infected with the viruses were treated with 10 μg/mL blasticidin (Invitrogen) for 3 days.

For the generation of cells depleted of endogenous Nbs1 and expressing ectopic Nbs1Wt-myc-His or Nbs1EDE-myc-His, HT29 cells expressing shNbs1 were infected with lentiviruses expressing pENTR1A Nbs1Wt-myc-His or pENTR1A Nbs1EDE-myc-His containing an shRNA-resistant mutation. Infected cells were treated with 10 μg/mL blasticidin and 2 μg/mL of puromycin (Sigma-Aldrich).

To express the inducible shRNA and gene, doxycycline (Sigma-Aldrich) was incubated in the medium at a concentration of 1 μg/mL for 3 days.

shRNA target sequences

The targeting sequences used in preparing shRNA were as follows: ATR, GCCGCTAATCTTCTAACATTA; CtIP, GCATCATCCTTCAGCCCTTGA; Nbs1, GGAGGAAGATGTCAATGTTAG; and control, CGTACGCGGAATACTTCGA.

Measurement of mitotic indices

Cells were treated with IR, UV, or MMS, and fixed with 70% ethanol at specific times. Nocodazole was added 1 hour after treatment. Fixed cells were then stained with antibodies to phospho-histone H3 at S10 (H3 pS10; 1:200; Millipore) for 1 hour, followed by 30-minute incubation with Alexa Fluor 488 secondary antibodies (1:100; Invitrogen). DNA was counterstained with 0.1 mg/mL propidium iodide containing RNase for 30 minutes at 37 °C. Flow cytometry was performed using a FACSCanto II flow cytometer (BD Biosciences).

Antibodies

Antibodies used in this study are listed in Supplementary Table S1.

Immunoblotting

For preparation of whole cell extracts, cells were lysed with immunoprecipitation kinase buffer (50 mmol/L HEPES, pH 8.0, 150 mmol/L NaCl, 2.5 mmol/L EGTA, 1 mmol/L EDTA 1 mmol/L DTT, 0.1% Tween 20, 10% glycerol) containing a cocktail of protease and phosphatase inhibitors. Cell lysates were boiled with SDS sample buffer (45 mmol/L Tris-HCl, pH 6.8, 10% glycerol, 1% SDS, 0.01% bromophenol blue, 50 mmol/L DTT). Proteins in the lysates were separated by SDS-PAGE and transferred onto polyvinylidene difluoride membranes. Membranes were incubated overnight with primary antibodies, followed by 1 hour incubation with horseradish peroxidase–conjugated secondary antibodies.

Immunoprecipitation

Immunoprecipitation was performed essentially as previously described (24). For immunoprecipitation, cells were lysed in immunoprecipitated kinase buffer containing a cocktail of protease and phosphatase inhibitors. Cell lysates were incubated with primary antibodies at 4 °C for overnight, followed by incubation with protein G-agarose (GE Healthcare) for 1 hour. Immunoprecipitates were thoroughly washed three times with immunoprecipitation kinase buffer and resuspended in 2× SDS sample buffer.

Immunohistochemical analysis

Cells on cover slips were fixed in 4% paraformaldehyde for 10 minutes at room temperature, permeabilized with 0.5% Triton X-100 in PBS for 10 minutes, and incubated in blocking buffer

Published OnlineFirst May 29, 2014; DOI: 10.1158/0008-5472.CAN-13-3604

(PBS + 5% bovine serum albumin + 0.1% Tween 20) for 30 minutes. The cells on the slips were then incubated with anti-RPA2 and anti-γ-H2AX antibodies diluted in blocking buffer (1:500) for 2 hours at room temperature, followed by incubation with anti-rat IgG conjugated with Alexa Fluor 488 (Life Technologies) and anti-rabbit IgG conjugated with Alexa Fluor 594 (Life Technologies) secondary antibodies diluted in blocking buffer (1:400) for 1 hour at room temperature. Nuclei were counterstained with Hoechst 33342 (1:1,000).

In vitro kinase assay

ATR kinase assays were performed essentially as previously described (25) with the following modifications. HEK293E cells were transfected with Flag-ATR– and His-ATRIP–expressing plasmids, and Flag-ATR was immunoprecipitated with anti-Flag M2 antibody in TGN buffer [50 mmol/L Tris-HCl (pH 7.5), 150 mmol/L NaCl, 50 mmol/L phosphoglycerol, 10% glycerol, 1% Tween 20, 1 mmol/L phenylmethylsulfonyl fluoride (PMSF), 1 mmol/L NaF, 1 mmol/L Na_3VO_4, 1 mmol/L DTT, and protease inhibitors]. The precipitates were washed twice with the TGN buffer, once with the TGN buffer supplemented with 0.5 M LiCl, and twice with the reaction buffer [10 mmol/L HEPES (pH 7.5), 50 mmol/L NaCl, 10 mmol/L $MgCl_2$, 50 mmol/L glycerophosphate, 1 mmol/L DTT, and protease inhibitors] without ATP. The *in vitro* kinase reactions were conducted in the presence of 50 μmol/L ATP and purified GST-Rad17. Phosphorylation of Rad17 was monitored using phospho-Rad17 (Ser645) antibody (Bethyl).

Preparation of nuclear extracts

HCT116 cells were grown to ≤80% confluence, trypsinized, and centrifuged (200 × *g* for 3 minutes at room temperature), then washed in PBS. The cell pellets were suspended in a 5× packed cell volume of hypotonic buffer A (10 mmol/L Hepes-KOH, pH 7.9, 10 mmol/L KCl, 1.5 mmol/L $MgCl_2$, 0.5 mmol/L DTT, and 0.5 mmol/L PMSF) supplemented with a cocktail of protease inhibitors (Nakalai Tesque) and incubated on ice for 5 minutes. Cells were then centrifuged at 500 × *g* for 5 minutes at 4°C, suspended in a 2× packed cell volume of buffer A and lysed by Dounce homogenization using a tight-fitting pestle. Nuclei were collected as a pellet by centrifugation at 4,000 × *g* for 5 minutes at 4°C and extracted in an equal volume of buffer C (20 mmol/L Hepes-KOH, pH 7.9, 600 mmol/L KCl, 1.5 mmol/L $MgCl_2$, 0.2 mmol/L EDTA, 25% glycerol, 0.5 mmol/L DTT, and 0.5 mmol/L PMSF) supplemented with a protease cocktail, and mixed on a rotator at 4°C for 30 minutes. Nuclear extracts (supernatants) were recovered by centrifugation (16,000 × *g* for 15 minutes at 4°C) and dialyzed using Slide-A-Lyzer Dialysis Cassettes (3,500-D protein molecular weight cutoff; Thermo Fisher Scientific) against buffer D (20 mmol/L Hepes-KOH, pH 7.9, 100 mmol/L KCl, 0.2 mmol/L EDTA, 20% glycerol, 0.5 mmol/L DTT, and 0.5 mmol/L PMSF). Dialyzed nuclear extracts were centrifuged (16,000 × *g* for 30 minutes at 4°C) to eliminate residual precipitates. The protein concentration of the clear supernatant was determined using Bradford's estimation method, and aliquots were snap frozen and stored at −80°C.

Extract-based ATR activation assay

An extract-based ATR activation assay was performed essentially as previously described (26) with the following modifications. Nuclear extracts were pretreated with 10 mmol/L of KU-55933 and NU7026 (Sigma-Aldrich) for 15 minutes on ice to inhibit ATM and DNA-PKcs, and supplemented with the reaction buffer (buffer R), which brought the final buffer compositions to 10 mmol/L HEPES (pH 7.6), 50 mmol/L KCl, 0.1 mmol/L $MgCl_2$, 1 mmol/L phenylmethanesulfonylfluoride, 0.5 mmol/L dithiothreitol, 1 mmol/L ATP, 10 mg/mL creatine kinase, and 5 mmol/L phosphocreatine. ssDNA (70nt) or ssDNA/dsDNA junction were incubated with the extracts for 15 minutes at 37 °C.

Sequences of DNA oligonucleotides

ss50: 5′-AGCGCCCAATACGCAAACCGCCTCTCCCCGCGC-GTTGGCCGA
TTCATTAA-3′
ss70: 5′-TGCAGCTGGCACGACAGGTTTTAATGAATCGG-CCAACGCGCG
GGGAGAGGCGGTTTGCGTATTGGGCGCT-3′.

Results

CBP-93872 specifically suppresses the DSB-induced G_2 checkpoint

To clarify the molecular basis of G_2 checkpoint abrogation by CBP-93872 (Fig. 1A), we first examined whether the effect of this drug on the G_2 checkpoint was dependent on the type of DNA damage. HT-29 cells lacking functional p53 were treated with IR, UV, or MMS in the presence or absence of CBP-93872, and the cell cycle before entry into mitosis arrest was evaluated by determining mitotic indices using phospho-histone H3 at serine 10 (H3 pS10) as a mitotic marker. CBP-93872 effectively suppressed G_2 arrest induced by IR treatment whereas it did not affect that induced by UV or MMS (Fig. 1B). In contrast, UCN-01 effectively suppressed G_2 arrest induced by UV and MMS. Consistent with this, upon IR treatment, Chk1 phosphorylation at serines 317 and 345 was notably compromised in the presence of CBP-93872 (Fig. 1C). Interestingly, CBP-93872 did not suppress ATM activation (phosphorylation of ATM at S1981; ATM pS1981) and subsequent phosphorylation of Chk2 after IR treatment. In addition, this drug did not affect Chk1 phosphorylation upon UV, MMS, or HU treatment (Fig. 1D–F). Taken together, these results suggested that the cellular target of CBP-93872 should exist downstream of DSB-induced ATM activation.

CBP-93872 does not inhibit initiation but does inhibit maintenance of the DSB-induced G_2 checkpoint

To examine the mode of G_2 checkpoint suppression by CBP-93872, we examined the percentage of H3 pS10-positive cells by flow cytometry. Mitotic indices, in the presence of CBP-93872, of HT29, A549, and NCI-H460 cells were significantly decreased at 1 hour after IR treatment, but increased at 16 hours (Fig. 2A). In contrast, reduction of these indices in the presence of caffeine or UCN-01 was only minimal at 1 hour and markedly increased at 12 hours. In MCF7 cells that possess functional

Published OnlineFirst May 29, 2014; DOI: 10.1158/0008-5472.CAN-13-3604

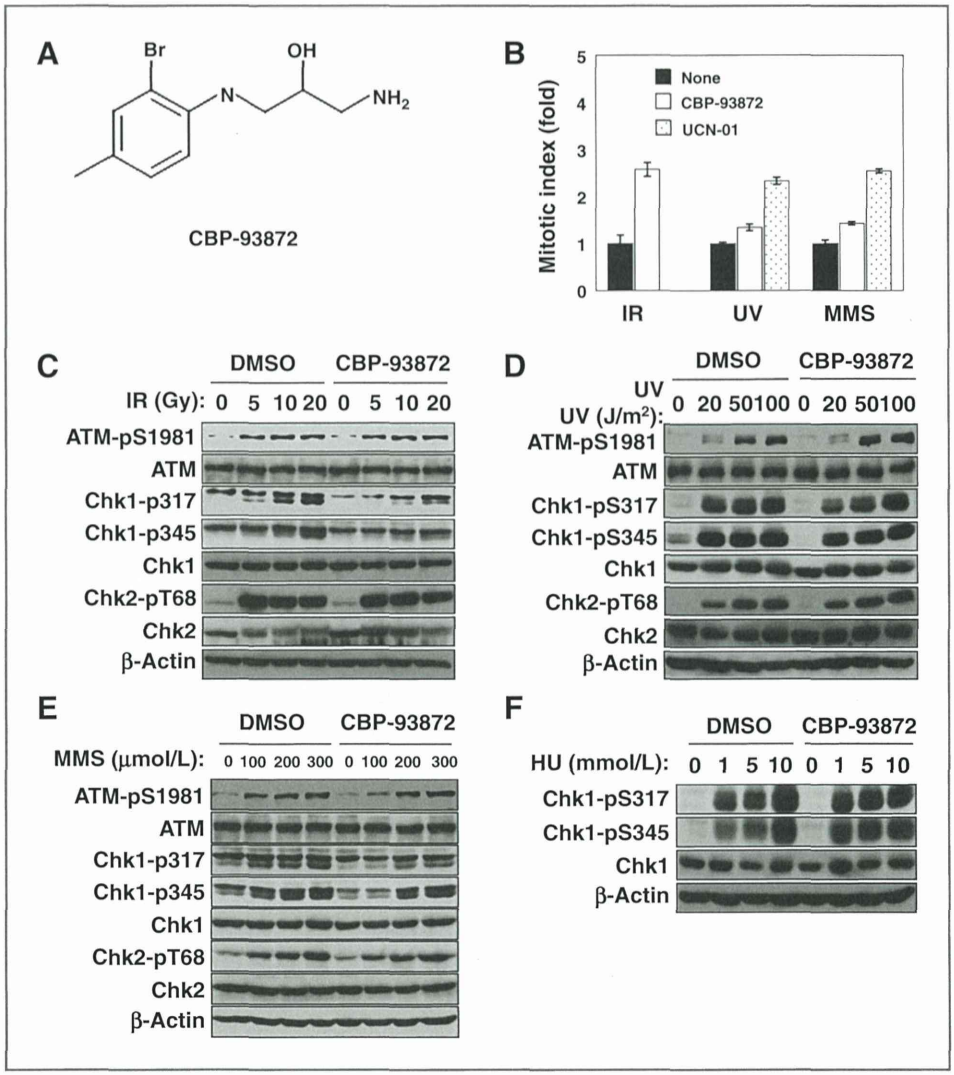

Figure 1. CBP-93872 specifically abrogated the IR-induced G_2 checkpoint. A, chemical structure of CBP-93872. B, HT29 cells were treated with IR (10 Gy), UV (10 J/m^2), or MMS (200 μmol/L). Eight hours after treatment, cells were then incubated in the presence or absence of CBP-93872 (20 μmol/L) or UCN01 (300 nmol/L). Nocodazole (500 nmol/L) was simultaneously added to prevent cells from exiting mitosis. Cells were fixed 8 hours after treatment and subjected to FACS analysis. Mitotic cells were determined to be positive for phospho-histone H3 at S10 (pS10) and relative mitotic indices are expressed as a multiple of those without inhibitors. Data are presented as means ± SD of at least three independent experiments. HT29 cells were treated with the indicated doses of IR (C), UV (D), MMS (E), or hydroxyurea (HU; F) in the presence or absence of CBP-93872 (20 μmol/L). Two hours (IR, UV, and MMS) or 4 hours (HU) after treatment, cells were harvested and whole cell extracts were subjected to immunoblotting using the indicated antibodies.

p53, mitotic indices in the presence of CBP-93872 were continuously low. These results suggested that CBP-93872 abrogates maintenance of the G_2 checkpoint, but not its initiation, whereas caffeine and UCN-01 inhibit both its initiation as well as its maintenance. Consistent with this, immunoblotting revealed that the level of H3 pS10 in the presence of CBP-93872 was reduced at 4 hours and was elevated again at 8 hours after IR treatment (Fig. 2B). In contrast, the levels of H3 pS10 were almost constant in the presence of UCN-01 and KU-55933, an ATM-specific inhibitor. As expected, KU-55933 inhibited IR-induced ATM pS1981 and subsequent phosphorylation of Chk2. UCN-01 did not inhibit IR-induced ATM pS1981 and Chk2 phosphorylation, but rather enhanced Chk1 phosphorylation at S317 and S345.

CBP-93872 suppresses DSB-induced ATR activation

We then examined whether CBP-93872 was inhibitory upstream or downstream of ATR activation. ATR activation was detected by its auto-phosphorylation at T1989 (25). Immunoblotting analysis revealed that phospho-ATR at T1989 as well as Chk1 phosphorylation were readily detected after doses of 1 Gy or more IR treatment (Fig. 3A). CBP-93872 strongly inhibited DSB-induced ATR activation and subsequent Chk1 phosphorylation. Importantly, UV treatment activated ATR in a dose-dependent manner and this activation as well as UV-induced Chk1 phosphorylation were not affected by the treatment with CBP-93872 (Fig. 3B). Treatment with CBP-93872 did not affect S-phase progression with or without UV treatment, eliminating the possibility that the inability of CBP-93872 to inhibit UV-induced Chk1 phosphorylation was an indirect consequence of an altered progression of S phase (Supplementary Fig. S1). We then examined whether CBP-93872 directly inhibited ATR activity. An *in vitro* kinase assay using recombinant wild-type ATR and ATRIP complex revealed that CBP-93872, even at a maximum concentration (200 μmol/L), failed to inhibit ATR activity whereas VE-821, an ATR-specific inhibitor, did so effectively, indicating that CBP-93872 is not a direct inhibitor of ATR (Fig. 3C). Taken together, a molecular target of CBP-93872 should exist during the process occurring between ATM-dependent

Published OnlineFirst May 29, 2014; DOI: 10.1158/0008-5472.CAN-13-3604

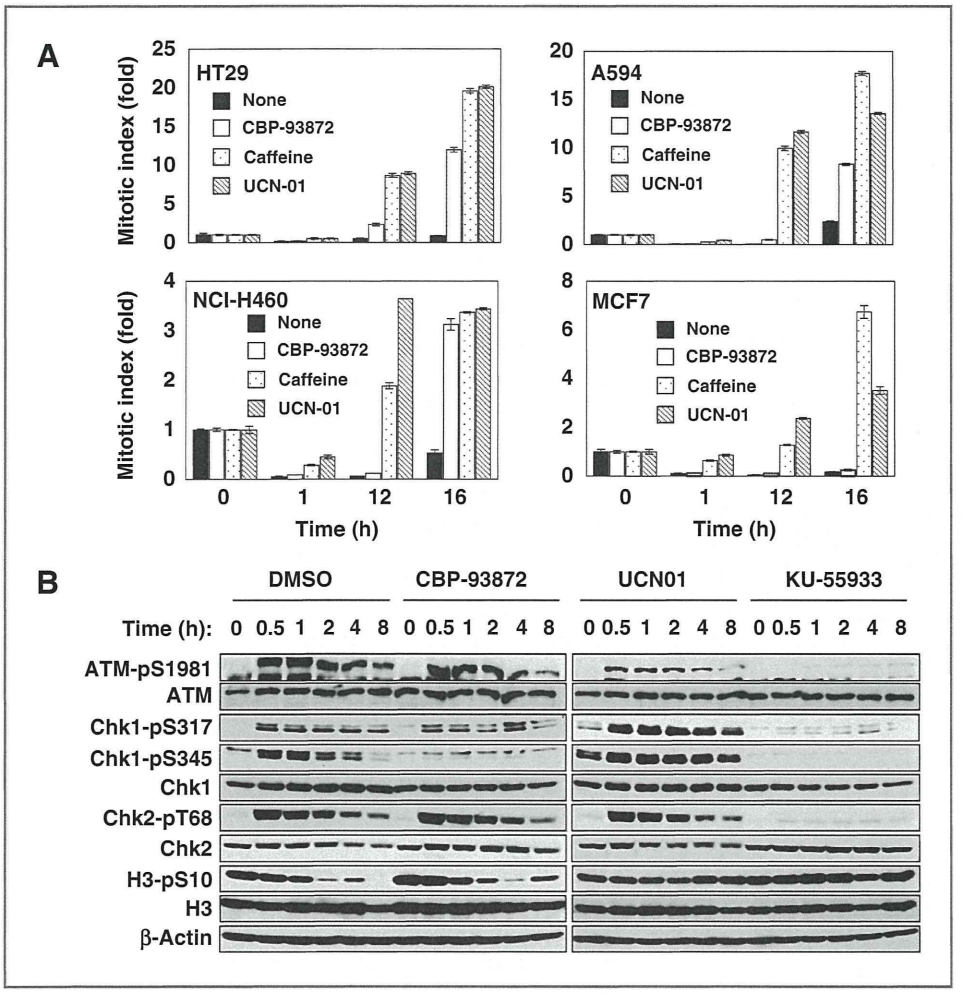

Figure 2. CBP-93872 abrogated maintenance, but not initiation, of the DSB-induced G_2 checkpoint. A, p53-deficient HT29, A549, and NCI-H460 cells and p53-positive MCF7 cells were treated with IR (10 Gy) in the presence of either DMSO (control), CBP-93872 (20 μmol/L), caffeine (2 mmol/L), or UCN01 (300 nmol/L). One hour after IR treatment, nocodazole (500 nmol/L) was added to cells as in Fig. 1B and cells were fixed at the indicated times. Fixed cells were then subjected to FACS analysis. Mitotic indices were determined as in Fig. 1B and data are presented as means ± SD of at least three independent experiments. B, HT29 cells were treated with IR (10 Gy) in the presence of DMSO (control), CBP-93872 (20 μmol/L), UCN01 (300 nmol/L), or KU-55933 (20 μmol/L). Cells were harvested at the indicated times after irradiation and whole cell extracts were subjected to immunoblotting using the indicated antibodies.

generation of the ATR-activating DNA structure and ATR activation.

CBP-93872 did not inhibit DNA-end resection at DSB sites

ATR activation in response to DSB requires conversion of ATM-activating DSB structures into ATR-activating structures (25, 26). DNA-ends at DSBs sites are rapidly processed by nucleases in combination with CtIP, generating ssDNA and a junction between ssDNA and dsDNA (27). ssDNA is bound by RPA, forming nuclear foci. Therefore, we used an immunohistochemical analysis using anti-RPA2 antibodies to determine whether CBP-93872 blocked DNA-end resection at DSB sites. In control cells, RPA2 foci formation was readily detectable after IR treatment. These nuclear foci were colocalized with γH2AX foci, suggesting that RPA2 foci represented ssDNA regions generated by DNA-end resection at DSB sites. Depletion of CtIP almost completely compromised RPA2 foci formation (Fig. 4A). In contrast, RPA2 foci were readily detectable in cells treated with CBP-93872. Interestingly, in response to DSB, depletion of CtIP showed an abrogation of the G_2 checkpoint similar to that upon treatment with CBP-93872 (28). Depletion of CtIP did not inhibit ATM autophosphorylation at S1981, but it did compromise Chk1 phosphorylation at S317 and S345 and RPA2 phosphorylation (Fig. 4B). As with the CBP-93872 treatment, DNA-end resection at DSB sites seemed to be required for maintenance of the G_2 checkpoint in response to DSB (Fig. 4C). These results suggested that molecular targets of CBP-93872 exist between DNA-end resection and ATR activation.

CBP-93872 inhibited ATR-dependent phosphorylation of Nbs1 at S343

Importantly, checkpoint activation, which is evaluated by Chk1 phosphorylation, seemed to be dependent on either Nbs1 or Rad17 depending on the type of DNA damage. On UV treatment, Chk1 phosphorylation at S317 and S345 was almost completely abrogated when Rad17, but not Nbs1, was depleted, whereas on IR treatment these phosphorylations were dependent on the presence of Nbs1 but not Rad17 (Supplementary Fig. S2). Treatment with CBP-93872 specifically inhibited NBS1-dependent, but not Rad17-dependent phosphorylation of Chk1 at S317 and S345 upon IR treatment, showing that the inhibitory effect of CBP-93872 was only a minimal in cells depleted of Nbs1. Consistent with this, 2 distinct modes of ATR activation have been recently proposed (29, 30). One is dependent on Rad17-TopBP1 circuitry and the other is dependent on the ssDNA-bound MRN complex. The former has been

Published OnlineFirst May 29, 2014; DOI: 10.1158/0008-5472.CAN-13-3604

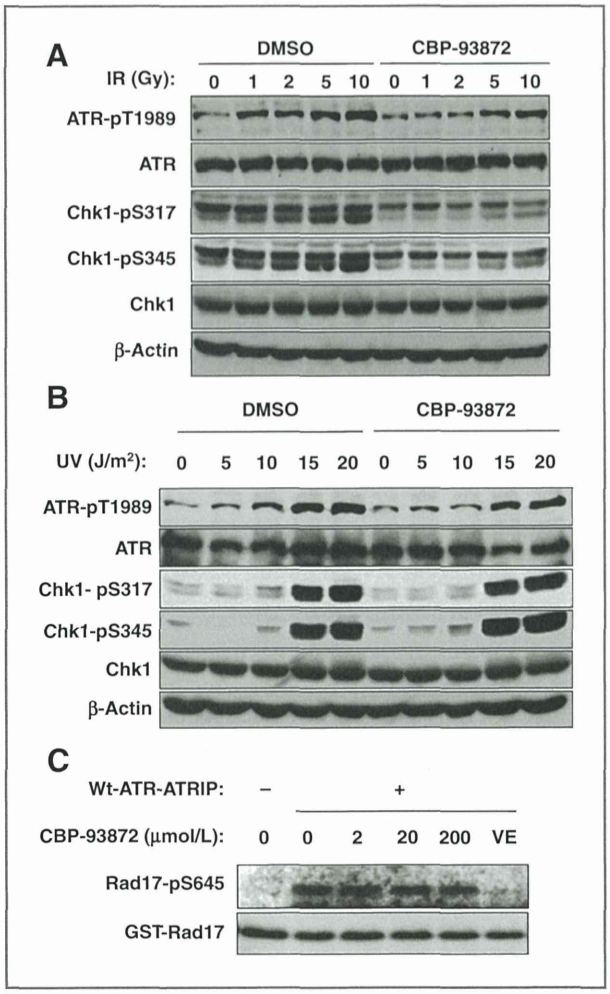

Figure 3. CBP-93872 specifically inhibited DSB-induced ATR activation. HT29 cells were treated with the indicated doses of IR (A) or UV (B) in the presence of DMSO or CBP-93872 (20 μmol/L). Cells were harvested at 2 hours after irradiation and WCEs were subjected to immunoblotting using the indicated antibodies. C, *in vitro* kinase assay using recombinant ATR-ATRIP complex and purified GST-Rad17 protein as a substrate. GST-Rad17 was incubated with or without purified wild-type-ATR-ATRIP (Wt-ATR-ATRIP) complex at 37°C for 30 minutes in the presence of the indicated concentration of CBP-93872 (20 μmol/L) or VE-821 (10 μmol/L). Kinase activity was stopped by boiling with SDS sample buffer, and phosphorylation of Rad17 at Ser645 was analyzed by immunoblotting using the specific antibodies (pRad17 Ser645).

proposed to be involved in mechanisms underlying initiation of ATR checkpoint signaling on a junction between ssDNA and double-stranded DNA, and the latter to be involved in the mechanism by which the ATR checkpoint signal is amplified on ssDNA. Therefore, we hypothesized that DSB-induced phosphorylation of Nbs1 at S343 was at least in part caused by activated ATR during amplification of the checkpoint signal. As shown in Fig. 5A, depletion of ATR strongly suppressed IR-induced Nbs1 phosphorylation at S343. Intriguingly, treatment with CBP-93872 also markedly inhibited this phosphorylation. Analysis of the kinetics of DSB-induced Nbs1 phosphorylation revealed that phosphorylation increased at 2 hours and reached a maximum at 4 to 8 hours, which was inhibited by CBP-93872 (Fig. 5B), suggesting that this phosphorylation is involved in the maintenance but not the initiation of the G_2 checkpoint. Importantly, CBP-93872 did not affect the complex formation of Nbs1 with Mre11 and Rad50 (Fig. 5B and C). CBP-93872 specifically inhibited IR-induced, but not UV-induced Nbs1 phosphorylation (Fig. 5C).

An Nbs1 mutant lacking RPA binding showed a defect in maintenance of the G_2 checkpoint

Given that RPA binding of Nbs1 is required for MRN-mediated ATR activation (29), we asked whether an Nbs1 mutant lacking RPA binding (EDE mutant) would exhibit a defect in the maintenance of the G_2 checkpoint as with CBP-93872 treatment. Depletion of Nbs1 resulted in the defect in initiation and maintenance of the G_2 checkpoint, as shown by the fact that the mitotic index was not decreased at 1 hour and was increased at 24 hours after IR treatment (Fig. 5D). Ectopic expression of wild-type Nbs1 in endogenous Nbs1-depleted cells restored the ability to arrest the cell cycle before mitosis, even at 24 hours after treatment. In contrast, as with CBP-93872 treatment, expression of the EDE mutant restored the ability to initiate G_2 arrest in response to DSB, but failed to maintain it. Consistent with this, as with CBP-93872 treatment, expression of the EDE mutant restored autophosphorylation of ATM (ATM pS1981) at 1 hour, but failed in phosphorylation of Chk1 at S345 at 24 hours (Fig. 5E). Complex formation of the EDE mutant with Mre11 and Rad50 was confirmed by immunoprecipitation-immunoblotting analysis using Mre11 immunoprecipitates (Fig. 5F). Taken together, these results indicated that a defect in MRN-dependent activation of ATR had a similar phenotype to that seen with CBP-93872 treatment.

CBP-93872 directly inhibited ssDNA-induced ATR activation *in vitro*

Finally, we examined whether CBP-93872 suppressed amplification of ATR checkpoint signaling on ssDNA or the ssDNA/dsDNA junction using a recently developed *in vitro* assay (29). In this system, ssDNA or the ssDNA/dsDNA junction alone when incubated with nuclear extract was sufficient to induce RPA2 S33 phosphorylation and this phosphorylation was dependent upon ATR, TopBP1, and Nbs1. CBP-93872 inhibited RPA2 phosphorylation at S33 in the nuclear extract incubated with ssDNA in a dose-dependent manner (Fig. 6A, left). However, CBP-93872 did not affect RPA phosphorylation at S33 in the extract incubated with the ssDNA/dsDNA junction (Fig. 6A, right). In addition, treatment with CBP-93872 in HT29 cells strongly suppressed RPA2 phosphorylation at S33 (Fig. 6B). Taken together, these results suggested that CBP-93872 directly inhibited amplification of ATR checkpoint signaling by suppressing ssDNA-dependent activation of ATR.

Discussion

Numerous G_2 checkpoint inhibitors have been developed and many have been proposed as potent candidates for DSB sensitization of p53-deficient cancer cells on the basis of the concept that survival of p53-mutated cancer cells relies on the

Published OnlineFirst May 29, 2014; DOI: 10.1158/0008-5472.CAN-13-3604

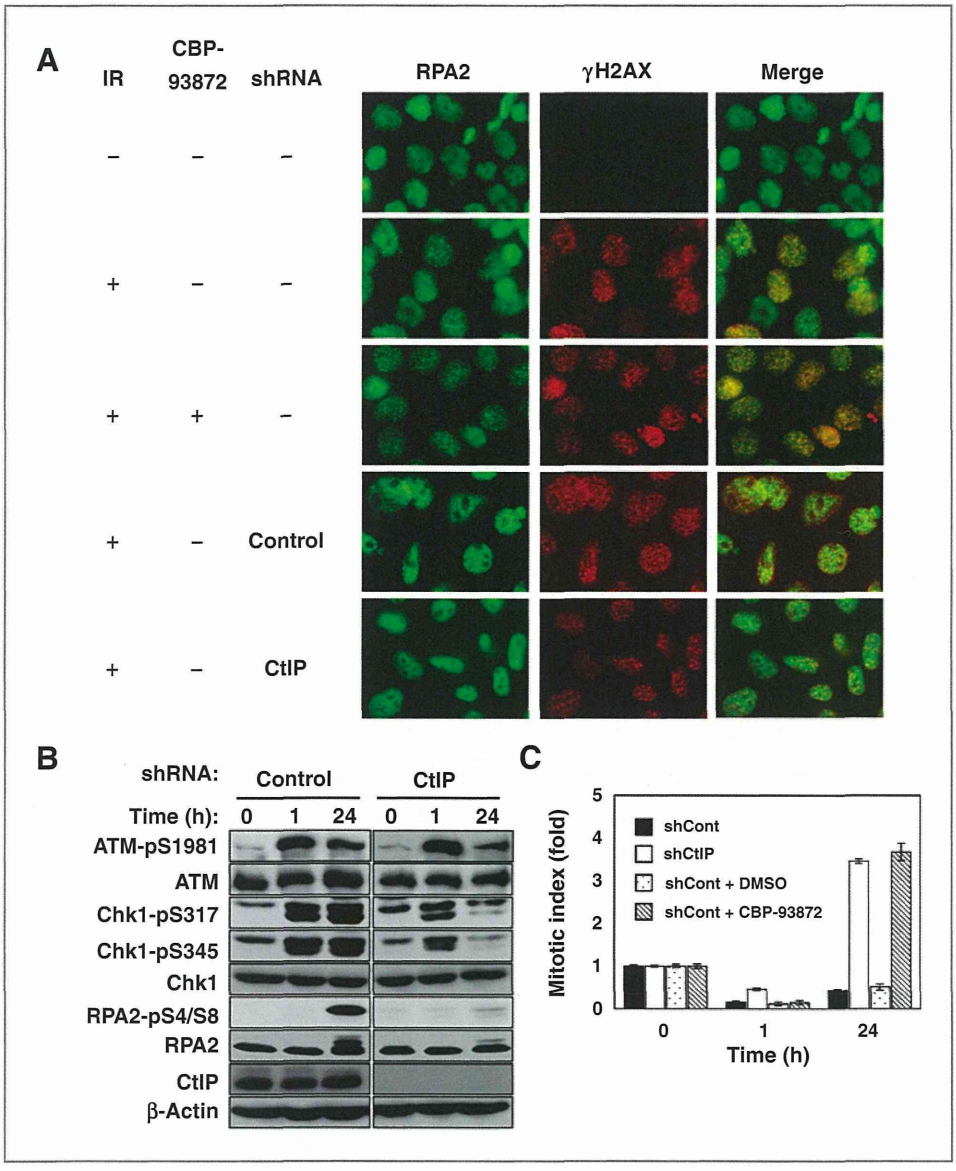

Figure 4. CBP-93872 did not affect IR-induced formation of RPA2 nuclear foci. A, HT29 cells were infected with Tet-on inducible lentiviruses expressing shControl or shCtIP. Infected cells were cultured in the presence of doxycycline (1 μg/mL) for 3 days. Cells were then treated with or without IR (10 Gy) in the presence or absence of CBP-93872 (20 μmol/L). Four hours after irradiation, cells were fixed and stained with anti-RPA2 and anti-γH2AX antibodies. Images were captured by fluorescence microscopy. Cells expressing shControl and shCtIP cells were irradiated with IR (10 Gy) as in A. Nocodazole (500 nmol/L) was added at 1 hour after IR and cells were collected at the indicated times. Whole cell extracts were subjected to immunoblotting using the indicated antibodies (B). Fixed cells were stained with anti-histone H3 pS10 antibodies and mitotic indices were determined as in Fig. 2A. Data are presented as means ± SD of at least three independent experiments (C).

Chk1-mediated G_2 checkpoint upon DSB. For example, Chk1 seems to be a promising target because this kinase is essential for G_2 arrest in response to various genotoxic stressors. Several small molecules exhibiting inhibitory activity toward Chk1 have been identified, such as UCN-01 (14). ATM and ATR are also candidates as targets of G_2 checkpoint inhibitors. In addition, a Wee1 inhibitor, MK-1775, has been developed as a potentiator of DNA damage caused by cytotoxic chemotherapy (31). However, the majority of these inhibitors interact with the ATP binding site of the kinase and it would be difficult to obtain highly selective ATP-competitive kinase inhibitors as the ATP binding site has a very similar structure in all kinases. Furthermore, in normal cells, most of their molecular targets play a key role in the survival and maintenance of genomic integrity. Therefore, these inhibitors can easily cause unexpected deleterious effects on normal cell function, diminishing the possibility of their clinical application.

To obtain G_2 checkpoint inhibitors with a novel mode of action, a high-throughput screening system using p53-deficient HT29 cells was used and CBP-93872 was identified as a potential candidate for use as a G_2 checkpoint inhibitor, although the molecular mechanisms underlying this inhibition are largely unknown. In this study, we found that CBP-93872 inhibited ATR activation specifically following DSB. ATR activation in response to DSB requires ATM activation and the subsequent processing of DSB ends by nucleases, generating ssDNA regions and ssDNA/dsDNA junctions that function as ATR-activating structures. Importantly, although ATR and ATM themselves play key roles in cell survival and maintenance of genomic integrity, respectively, during the normal cell cycle (19, 22), the molecular pathway between ATM activation and ATR activation seems not to be essential for normal cell growth. Therefore, molecules that target this pathway would be most the desirable for use as drugs, because they have far

Published OnlineFirst May 29, 2014; DOI: 10.1158/0008-5472.CAN-13-3604

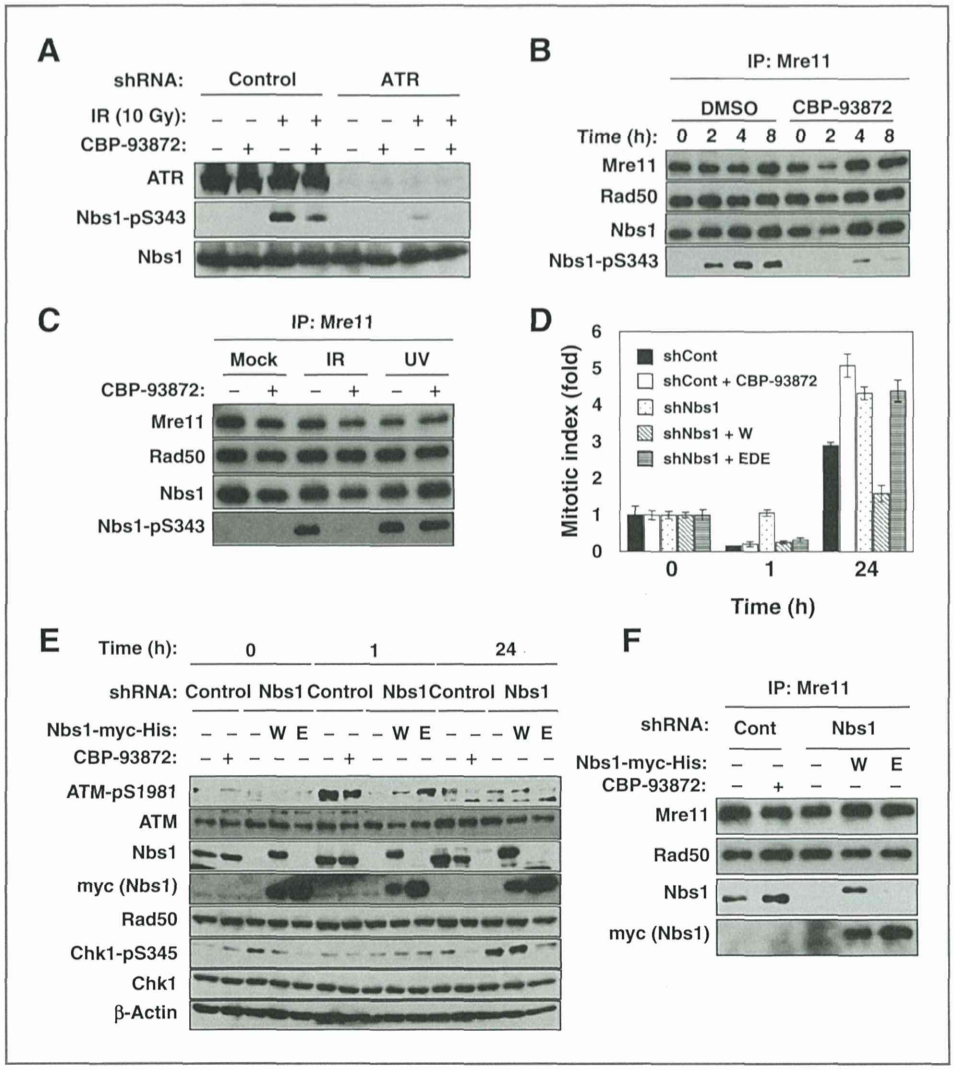

Figure 5. CBP-93872 inhibited ATR-mediated Nbs1 phosphorylation at S343, and a mutant Nbs1 lacking the ability to bind to RPA2 showed a similar G_2 checkpoint abrogation to that with CBP-93872 treatment. A, HT29 cells were infected with Tet-on inducible lentiviruses expressing shControl or shATR. These cells were cultured in the presence of doxycycline (1 μg/mL) for 3 days. Cells were treated with or without IR (10 Gy) in the presence or absence of CBP-93872 (20 μmol/L). Two hours after irradiation, cells were harvested and the chromatin fractions were analyzed by immunoblotting using the indicated antibodies. B, HT29 cells were exposed to IR (10 Gy) in the presence of DMSO (control) or CBP-93872 (20 μmol/L) and harvested at the indicated times. Cell lysates were immunoprecipitated using anti-Mre11 antibodies. The resultant immunoprecipitates were subjected to immunoblotting using the indicated antibodies. C, HT29 cells were mock treated or treated with IR (10 Gy) or UV (100 J/m^2) in the presence or absence of CBP-93872 (20 μmol/L). Cells were harvested 2 hours after IR treatment. Immunoprecipitation and immunoblotting were performed as in B. D, HT29 cells expressing control shRNA (Control) or cells depleted of endogenous Nbs1 (Nbs1) were transfected with plasmids expressing myc-tagged Nbs1, either wild-type (W) or an EDE mutant (E) that lacks the ability to bind to RPA2. Cells were treated with IR and mitotic indices were determined as in Fig. 2A. Data are presented as means ± SD of at least three independent experiments. E, cells were treated with IR (10 Gy) in the presence or absence of CBP-93872 (20 μmol/L). One hour after irradiation, nocodazole (500 nmol/L) was added and cells were harvested at the indicated times. The lysates were subjected to immunoblotting using the indicated antibodies. F, cell lysates from HT29 cells expressing either wild-type or an EDE mutant Nbs1 were immunoprecipitated using anti-Mre11 antibodies. The resultant immunoprecipitates were subjected to immunoblotting using the indicated antibodies.

less cytotoxicity and possess the ability to potentiate the antitumor efficiency of DNA-damaging agents.

Very recently, it was reported that ATR activation following DSB is regulated by two distinct modes (29, 30). After DNA-end resection is initiated, the Rad17–RFC complex recognizes generated ssDNA/dsDNA junctions and subsequently recruits Rad9–Rad1–Hus1 (9-1-1) complexes and TopBP1 onto the junctions. This recruitment leads to the initiation of ATR activation. Continued DNA-end resection results in lengthened ssDNA regions that recruit RPA and ATR-ATRIP. MRN complexes then directly bind to RPA-ssDNA through the EDE domain of Nbs1 and recruit TopBP1, activating ATR-ATRIP. This mode of action seems to function in the amplification and maintenance of ATR checkpoint signaling (32). CBP-93872 specifically inhibited maintenance, but not initiation, of ATR checkpoint signaling, suggesting that it functions in Nbs1-dependent ATR activation (Fig. 6C). Intriguingly, CBP-93872 directly inhibited ssDNA-induced but not ssDNA/dsDNA

Published OnlineFirst May 29, 2014; DOI: 10.1158/0008-5472.CAN-13-3604

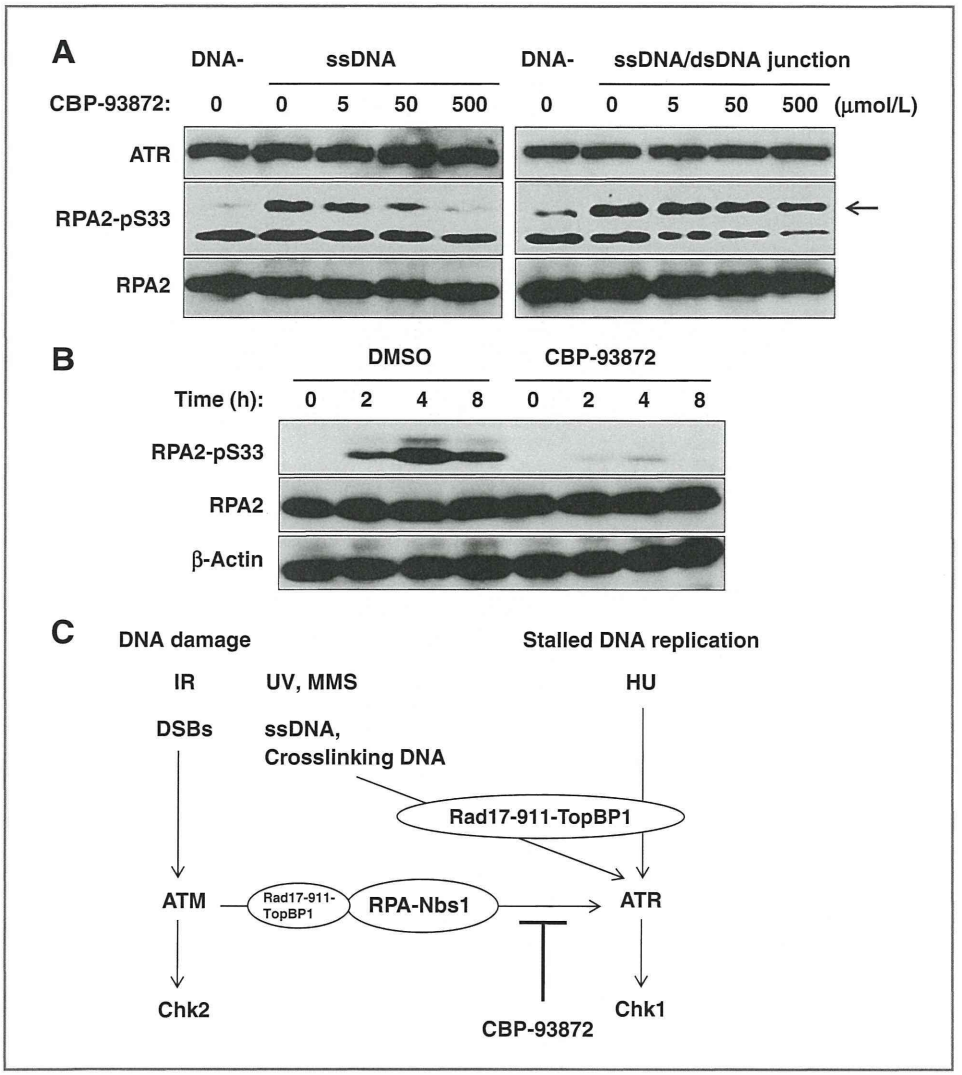

Figure 6. CBP-93872 inhibited ssDNA-dependent ATR activation *in vitro*. A, nuclear extracts prepared from HCT116 cells were incubated with 70nt single-stranded DNA (ssDNA) or ssDNA/dsDNA junction produced by annealing 70nt ssDNA with 50nt ssDNA at 37°C for 15 minutes. The extracts were then subjected to immunoblotting and phosphorylation of RPA2 pS33 was detected with the specific antibodies. The arrows indicate phosphorylation bands of RPA2 at S33. B, HT29 cells were treated with IR (10 Gy) in the presence of DMSO or CBP-93872 (20 μmol/L). Cells were harvested at the indicated times and the lysates were subjected to immunoblotting using the indicated antibodies. C, schematical presentation of the molecular basis underlying checkpoint inhibition by CBP-93872. ATR activation following DSB is regulated by two distinct modes. After DNA-end resection is initiated, Rad17-(9-1-1)-TopBP1 leads to the initiation of ATR activation. Continued DNA-end resection recruits RPA–Nbs1 complexes and further activates ATR. ATR activation following ssDNA or cross-linking DNA generated by DNA damage or stalled DNA replication is mainly mediated by the Rad17-(9-1-1)-TopBP1 axis independently of Nbs1. In this way, CBP-93872 specifically inhibits Nbs1-dependent ATR activation.

junction activation of ATR *in vitro*. Consistent with this, treatment with CBP-93872 suppressed ATR-dependent Nbs1 phosphorylation at S343 and RPA2 phosphorylation at S33.

In conclusion, although the detailed mechanism underlying inhibition of ssDNA-induced ATR activation by CBP-93872, including its structural basis, remains elusive, our results showed that ssDNA-induced ATR activation is a promising molecular target for a G_2 checkpoint inhibitor that specifically sensitizes p53-mutated cancer cells to DSB-inducing DNA damage therapy.

Disclosure of Potential Conflicts of Interest

No potential conflicts of interest were disclosed.

Authors' Contributions

Conception and design: M. Nakanishi
Development of methodology: T. Hirokawa
Acquisition of data (provided animals, acquired and managed patients, provided facilities, etc.): T. Hirokawa, B. Shiotani, K. Murata, Y. Johmura, M. Haruta
Analysis and interpretation of data (e.g., statistical analysis, biostatistics, computational analysis): T. Hirokawa, B. Shiotani, M. Shimada, K. Murata, M. Haruta, H. Tahara, H. Takeyama
Writing, review, and/or revision of the manuscript: T. Hirokawa, M. Nakanishi
Administrative, technical, or material support (i.e., reporting or organizing data, constructing databases): B. Shiotani, M. Shimada, M. Nakanishi
Study supervision: M. Nakanishi

Acknowledgments

The authors thank Dr. N. Harada and Chugai Pharmaceutical Co., Ltd. for providing CBP-93872 and Dr. H. Miyoshi for lentiviral vectors. The authors thank Y. Chiba and C. Yamada-Namikawa for technical assistance.

Grant Support

This work was performed as a research program of the Project for Development of Innovative Research on Cancer Therapeutics (P-DIRECT), Ministry of Education, Culture, Sports, Science and Technology of Japan (M. Nakanishi). This work was also supported by a Grant-in-Aid for Scientific Research on Innovative Area "Cell fate control," Scientific Research (A), and Challenging Exploratory Research from the Ministry of Education, Culture, Sports, Science and Technology of Japan (M. Nakanishi).

The costs of publication of this article were defrayed in part by the payment of page charges. This article must therefore be hereby marked *advertisement* in accordance with 18 U.S.C. Section 1734 solely to indicate this fact.

Received December 20, 2013; revised April 10, 2014; accepted April 17, 2014; published OnlineFirst May 29, 2014.